Water-Dispersible, Multifunctional, Magnetic, Luminescent Silica-Encapsulated Composite Nanotubes

*Hongjun Zhou, Jingyi Chen, Eli Sutter, Mikhail Feygenson, M. C. Aronson, and Stanislaus S. Wong**

***A** multifunctional one-dimensional nanostructure incorporating both CdSe quantum dots (QDs) and Fe_3O_4 nanoparticles (NPs) within a SiO_2-nanotube matrix is successfully synthesized based on the self-assembly of preformed functional NPs, allowing for control over the size and amount of NPs contained within the composite nanostructures. This specific nanostructure is distinctive because both the favorable photoluminescent and magnetic properties of QD and NP building blocks are incorporated and retained within the final silica-based composite, thus rendering it susceptible to both magnetic guidance and optical tracking. Moreover, the resulting hydrophilic nanocomposites are found to easily enter into the interiors of HeLa cells without damage, thereby highlighting their capability not only as fluorescent probes but also as possible drug-delivery vehicles of interest in nanobiotechnology.*

Keywords:
- cadmium selenide
- composite nanotubes
- encapsulation
- photoluminescence
- silica

[*] H. Zhou,[†] S. S. Wong
Department of Chemistry
State University of New York at Stony Brook
Stony Brook, NY 11794 (USA)
E-mail: sswong@notes.cc.sunysb.edu

J. Chen,[+] M. Feygenson, M. C. Aronson, S. S. Wong
Condensed Matter Physics and Materials Sciences Department
Brookhaven National Laboratory
Building 480, Upton, NY 11973 (USA)
E-mail: sswong@bnl.gov

E. Sutter
Center for Functional Nanomaterials
Brookhaven National Laboratory
Building 735, Upton, NY 11973 (USA)

M. C. Aronson
Department of Physics
State University of New York at Stony Brook
Stony Brook, NY 11794 (USA)

[†] Current address: Department of Chemistry & Biochemistry
The University of Texas at Austin
Austin, TX 78712-0165 (USA)

[+] Current address: Department of Biomedical Engineering
Whitaker Hall, Washington University
St. Louis, MO 63130 (USA)

Supporting Information is available on the WWW under http://www.small-journal.com or from the author.

DOI: 10.1002/smll.200901276

1. Introduction

The translational trajectory of nanomaterials from a matter of basic, fundamental research to that of serious, practical applicability has become a focal point of increasing interest over the years. Specifically, biologically functionalized nanoparticles (NPs) have been used for a host of relevant biomedical applications including biolabeling, imaging, tumor targeting (such as enzyme encapsulation for therapy), diagnostics, optical sensing, biosensors, protein detection, drug delivery, and contrast enhancement in magnetic resonance imaging (MRI).[1,2]

Indeed, NPs for biology need to be surface functionalized, not only to render them both reasonably water soluble and buffer stable, but also to provide active sites for subsequent functional conjugation with biological moieties. Apart from ligand exchange and cross-coupling reactions, the choice of a silica shell coating as a passivating layer has become one of the more popular strategies for modifying the surfaces of NPs.[3–5] For instance, silica encapsulation of metal clusters and quantum dots (QDs) does not appear to perturb their core optical properties but, rather, prevents their aggregation, coagulation, and photochemical degradation.[6,7] In addition, silica is relatively biocompatible and its thickness can be tuned with nanometer precision.[8] Moreover, silica contains free silanol

NANO MICRO small

groups that can be subsequently reacted with additional appropriate functional groups through relevant silanization reactions.[9,10]

An interesting variation on this theme has been the development of silica encapsulation of NPs with dual functionalities, such as fluorescence/photostability and magnetism.[11] Such materials can be physically manipulated through the application of an external magnetic field and simultaneously optically probed by monitoring their fluorescence in real time. To take this idea one step further, it has recently been proposed that preformed nanocrystals could themselves be used as both magnetic and optical subunits in these silica core–shell systems. Specifically, superparamagnetic iron oxide NPs have been used for magnetism-based protein harvesting, MRI, hyperthermia treatment, bioseparation, and magnetic sensing of biomolecules,[12,13] while semiconducting QDs have been used in fluorescence-based biolabeling and imaging applications at the subcellular level.[14] Interestingly, magnetic properties, such as blocking temperatures, coercivities, and magnetization values in magnetite NPs, have been found to depend on size.[15] Moreover, as compared with either conventional organic dyes or lanthanide metal complexes, QDs offer high photostability, good fluorescence efficiency, broad excitation spectra, narrow emission-band widths with emission wavelengths directly correlated to particle sizes, and, finally, a large two-photon-absorption cross section.[16]

Several approaches have been attempted to achieve this synthetic objective via zero-dimensional (0D)-NP-composite formation and are extensively discussed in the Supporting Information. Nonetheless, the complementary 1D analogues of these multifunctional silica-based composites have not been reported as extensively.[17–22] The interest in 1D nanostructures arises from their unique shape-dependent properties, allowing for their use as building blocks in the assembly of a range of functional devices.[23,24] In the specific context of drug delivery and biomedicine, it is known that shape often plays a decisive role.[25] For instance, the internalization of rod-like, high-aspect-ratio hydrogel particles in HeLa cells was found to occur significantly faster and more efficiently than their spherical counterparts.[26] There are many advantages to using uniform silica nanotubes as the template in which to incorporate QDs and NPs.[18,27] First, nanotubes possess inner voids that can be filled with a variety of species ranging in size from large proteins to small molecules. Second, these nanotubes have spatially distinctive inner and outer surfaces that can, in theory, be differentially functionalized. Third, the dimensions of these silica nanotubes can be controlled. Fourth, the template technology used to generate these silica nanotubes is sufficiently robust and flexible that nanotubes possessing any desired physicochemical property, such as biodegradability, can be rationally designed.

The novelty of the approach described in this Full Paper relies on its fundamental simplicity. We have inserted preformed, monodisperse magnetic Fe_3O_4 NPs and luminescent CdSe QDs to the inner surface, preferentially functionalized by a hydrophobic coating, of a silica-nanotube template through noncovalent interactions. This ''insertion'' reaction did not involve either ligand exchange, strong acid or base, or high-temperature steps. Hence, our as-created 1D silica nanocomposite possessed not only the distinctive magnetic profile of Fe_3O_4 (useful for guided delivery) but also the desirable optical signature of CdSe (important for tracking). Furthermore, the structural integrity of these functional NPs was preserved and retained within the silica nanotube's outer shell, thereby offering a protective layer against local environmental influences. What is even more intriguing is that the outer silica surface could itself act as a reactive platform on which to graft additional moieties, such as biomolecules. Finally, our silica-nanotube constructs are reasonably monodisperse in size and shape, which can sometimes be difficult to achieve in the synthesis of as-prepared magnetic, luminescent silica beads.[11]

2. Results and Discussion

2.1. Structural and Optical Characterization

The crystallographic phase of our resulting silica-encapsulated nanocomposite was examined by X-ray diffraction (XRD) and is shown in Figure 1A. We have also included data on our constituent nanostructures, namely as-prepared CdSe QDs (Joint Committee on Powder Diffraction Standards (JCPDS) #19-0191) and Fe_3O_4 NPs (JCPDS #19-0629). Peaks for all materials appear to be broadened, as would be expected of small nanomaterials in comparison with their larger bulk analogues. Though the magnetite peaks are prominent, there is no peak that can be obviously ascribed to SiO_2 and CdSe in the resulting pattern of the composite. The absence of a distinctive SiO_2 peak and the broadness of the profile may be due to the amorphous nature of the silica nanotube itself, which has been noted previously.[28,29] The absence of the CdSe peak may potentially be attributed to the limited amount of CdSe QDs incorporated into the silica nanotubes. To ensure biocompatibility, we intentionally lowered the concentration of CdSe QDs versus that of Fe_3O_4 NPs in the final composite because of the potential issue of CdSe toxicity. In the final product, the concentration of CdSe was optimized to ensure detection under normal fluorescence conditions.

The optical UV/Vis absorption spectra of our as-prepared samples are shown in Figure 1B. Our amorphous silica-nanotube template does not possess a noticeable peak in the region of 300–800 nm, in agreement with prior data on porous hollow silica nanotubes.[30] CdSe QDs possess a strong absorption peak at around 550 nm, which corresponds to a

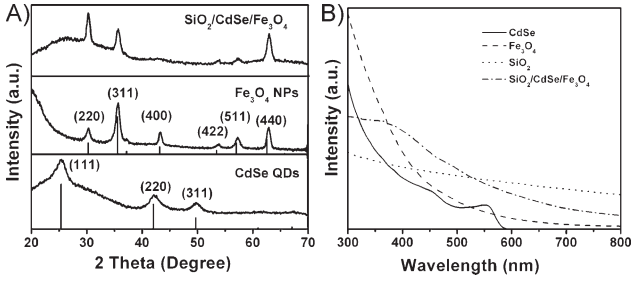

Figure 1. A) XRD patterns of CdSe QDs, Fe_3O_4 NPs, and silica-encapsulated composites. B) Corresponding UV/Vis spectra of CdSe QDs, Fe_3O_4 NPs, silica nanotubes, and silica-encapsulated composites.

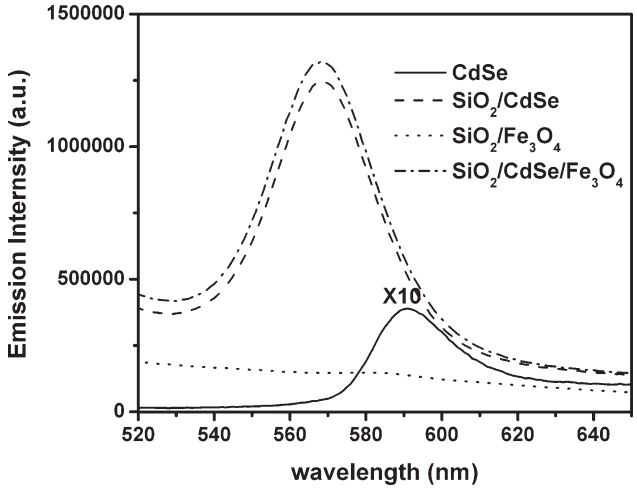

Figure 2. Room-temperature PL emission spectra ($\lambda_{ex} = 488$ nm) of bare CdSe QDs, as well as silica-encapsulated CdSe, silica-encapsulated Fe_3O_4, and silica-nanotube composites incorporating both CdSe and Fe_3O_4 nanocrystals.

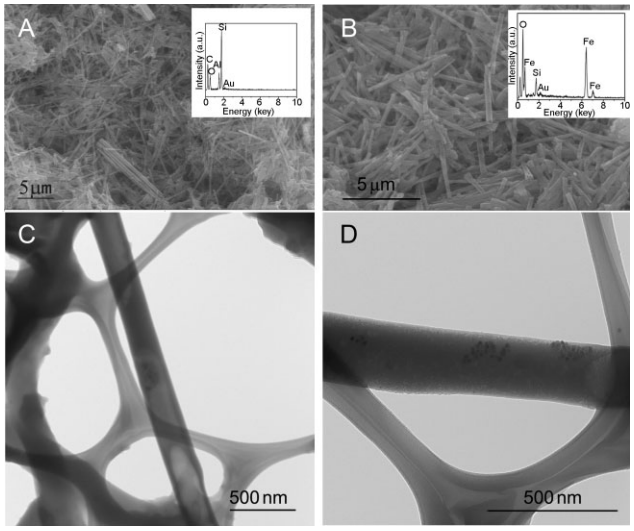

Figure 3. Scanning electron microscopy (SEM) and transmission electron microscopy (TEM) images of A,C) SiO_2 nanotubes and B,D) SiO_2/CdSe/Fe_3O_4-composite nanostructures. Insets of (A) and (B) highlight the EDS spectra of Au-coated samples of these materials. The presence of carbon can be ascribed to contamination in the SEM system sample chamber.

mean size of 3 nm, in expected agreement with our synthetic protocol.[31] Due to the low concentration of CdSe QDs, this peak was not obviously present in the composite spectrum. By contrast, the broad, essentially featureless signal due to Fe_3O_4 can be ascribed to the fact that it is an indirect-bandgap semiconductor.[32] Nonetheless, a very weak shoulder in the silica composite spectrum at 470 nm is in agreement with prior observations on analogous nanocomposites.[33–35]

Figure 2 highlights the room-temperature photoluminescence (PL) spectra of isolated CdSe QDs, silica-encapsulated CdSe, silica-encapsulated Fe_3O_4, and silica nanotubes containing both CdSe and Fe_3O_4 nanocrystals. The presence of an emission peak of pristine CdSe QDs in cyclohexane solution at around 590 nm was noted, in general agreement with that previously reported;[31] the weakness of the peak, however, has previously been ascribed to the exposure of surface defects associated with the nature and composition of the dispersing medium.[36] While there was an absence of any peak in the silica-encapsulated Fe_3O_4 sample, as expected, a peak at around 570 nm in water was noted not only for silica-encapsulated CdSe but also for silica nanotubes containing both CdSe and Fe_3O_4 nanocrystals. Though the emission peak remained symmetric without a red tail, the signal was clearly blueshifted and broadened as compared with that of bare CdSe, an observation that has been definitively noted with analogous silica-encapsulated systems.[13,16,37] One possible suggested reason is that the QDs may have undergone ligand removal and ''surface corrosion'' during the encapsulation process, leaving the QDs unprotected.[38] Our observation of emission peaks in all silica-nanotube samples incorporating CdSe suggests that the optical properties of CdSe QDs remained intact even after insertion into silica, thereby rendering these composite structures as legitimate luminescent imaging probes.

Sample morphology was ascertained by means of electron microscopy measurements (Figure 3) on Au-coated samples. The diameters of the as-prepared silica nanotubes (Figure 3A and C) were in the range of $\approx 220 \pm 40$ nm with lengths of $\approx 4.5 \pm 1.5$ μm. As is apparent from the data, there was no obvious change in the silica-nanotube morphology, even after the incorporation of discrete functional NPs (Figure 3B and D). Not surprisingly, the energy dispersive X-ray spectrum (inset of Figure 3A) of the silica nanotube alone evinced the presence of Si in addition to Al and O signals originating from the Al template residue. By contrast, the corresponding data (inset of Figure 3b) for the silica-encapsulated composite showed an expected Si signal as well as a number of Fe peaks, though no peaks clearly attributable to Cd and Se were observed. This absence of Cd and Se peaks in our composite sample was mainly due to the relatively low concentration of CdSe as compared with Fe_3O_4.

Analytical high-resolution transmission electron microscopy (HRTEM) techniques were utilized to obtain further structural insights into the nature of our samples. An isolated silica-nanotube control sample, in the absence of Fe_3O_4 and CdSe, is shown in Figure 4A and B. This material is clearly open at its end and its surface texture is morphologically distinctive from that of our nanocomposites, which is shown subsequently in Figure 4C–F. That is, bright-field (BF) and high-angle angular dark field (HAADF) scanning TEM (STEM) images are presented in Figure 4C and D, respectively. Higher-magnification BF and Z-contrast images are shown in Figure 4E and F. As expected, it is apparent from this data that there is a discernible contrast between the nanotubes and the two differently sized NPs, reflective of variations in the chemical composition (atomic number (Z)) of these materials. Localized energy-dispersive X-ray spectroscopy (EDS) data at specific NP sites on the silica-nanotube surface were obtained using a 0.2-nm beam in STEM mode and the corresponding data is shown in Figure 4G. Briefly, the presence of Cd was noted with the smaller NPs (blue curve), whereas the Fe signal was associated with the larger NPs (red curve), confirming the

NANO MICRO small

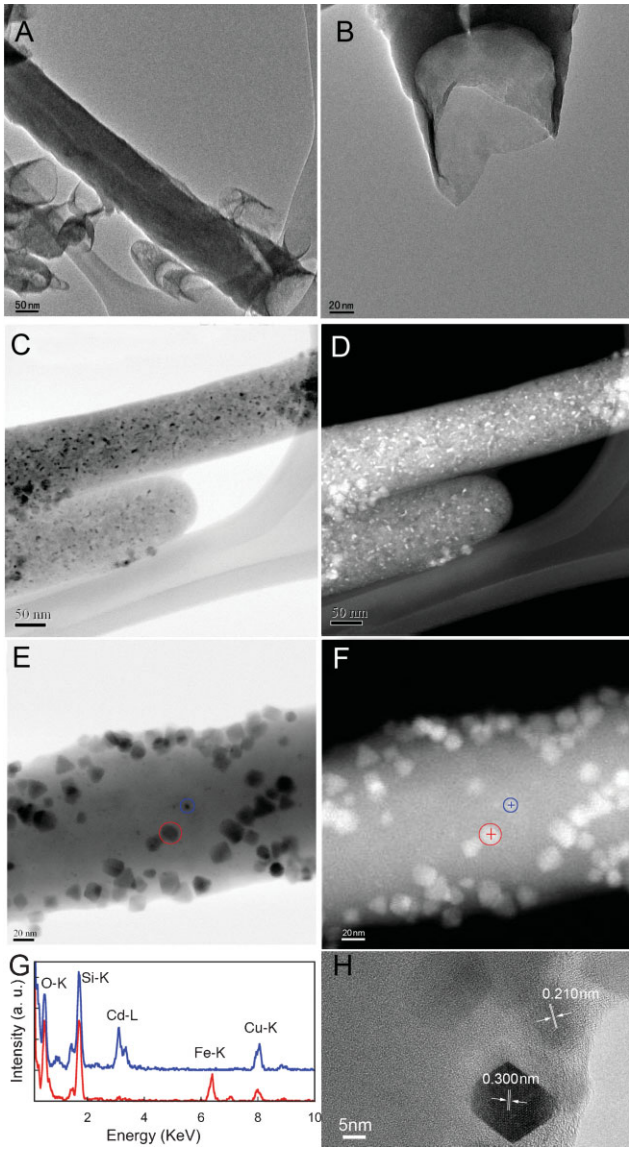

Figure 4. Control experiment: A,B) BF STEM images of silica nanotubes. Opened ends of selected nanotubes are shown. Desired product: C,E) BF STEM image, D,F) HAADF STEM image, G) EDS spectra, and H) HRTEM image of a silica-encapsulated CdSe/Fe_3O_4-composite nanostructure. Individual spectra in (G) are associated with data taken at red and blue cross sites, respectively, which are spatially highlighted in (F).

presence of CdSe QDs and Fe_3O_4 NPs associated with this SiO_2-nanotube matrix. The determination of the lattice dimensions obtained from the HRTEM image (Figure 4H) further supports this assertion. Specifically, measured *d* spacings, taken from adjacent nanocrystalline structures, can be attributed to the (220) planes of CdSe (0.210 nm) and Fe_3O_4 (0.300 nm), respectively.

We should mention that these 0D nanostructures were solidly bound to our silica 1D matrix, even after extensive washing, without evident property dilution. Based on our microscopy analysis, the loading density of our NPs was noted to be ≈24 Fe_3O_4 NPs and ≈4 CdSe QDs per 100 nm of silica-nanotube surface, though these values could be altered by rational manipulation of the particle concentrations. In the Supporting Information (Figures S4 and S5), we have demonstrated that we can independently vary the amounts and ratio of CdSe and/or Fe_3O_4 NPs incorporated into our silica nanotube by judiciously controlling either the immersion time (up to 24 h) or the actual NP concentration (up to 250 mM). As such, we found that, if needed, we could load as much as 3% of CdSe and 0.4% of Fe_3O_4 of the initial reagent NP solution into the final silica-based composite product. Nonetheless, as previously mentioned, we had deliberately decreased the amount of CdSe used in order to minimize the potential toxicity of the overall composite nanostructure while conserving its favorable optical properties. Moreover, silica encapsulation of CdSe has been found to decrease its inherent toxicity.[39]

Though Figure S6, a low-magnification view of the area surrounding Figure 4H, clearly highlights the presence of the silica outer coating definitively encapsulating iron oxide NPs and QDs, our cumulative data cannot be used to support the notion that all of the NPs and QDs were immobilized entirely within the silica-nanotube matrix itself. The apparent presence of crystalline NPs localized on and embedded within the external amorphous silica-nanotube surface may have been due to a number of factors, including the very small thickness (e.g., the distance between inner and outer shells) of the silica nanotube itself, which is apparent in Figure 4B. In fact, it measures ≈10 nm, which is consistent with the expected sheath thickness for the SiO_2 nanotube in the protocol that we utilized.[40] Nonetheless, this size is either on the order of magnitude of or even smaller than some of the reagent NPs themselves, which would lead to potential difficulty in spatially differentiating between these various nanostructures, even with microscopy. Moreover, if the observed as-prepared silica-nanotube diameter was even slightly smaller than that of the alumina-template pore channel itself, which is a very reasonable assumption based on the statistical range of our measurements, then the silane and NP reagents would, therefore, have reacted with both the external and internal nanotube surfaces, again explaining our data.

2.2. Insights Into Magnetic Behavior

On a macroscopic level, to demonstrate that the composites were noticeably magnetic, we confirmed that the behavior of a suspension of our multifunctional Fe_3O_4-based, luminescent, silica-encapsulated composite nanotubes was highly responsive to the movement of an external magnetic field of limited strength (Figure S7). The magnetic properties of our as-prepared silica-composite structures were more precisely measured using a superconducting quantum interference device (SQUID) magnetometer.

Figure 5 shows the magnetization as a function of the applied magnetic field at 30 and 300 K for both samples. They both show a small coercive field at 30 K, which becomes negligible at 300 K (Figure 5B and D). This indicates a clear transition from ferri- or ferromagnetism below the blocking temperature to superparamagnetism at high temperatures, which is characteristic of superparamagnetic NPs.[41]

We note the significant reduction of the saturation magnetization of Fe_3O_4/CdSe silica-based composites as

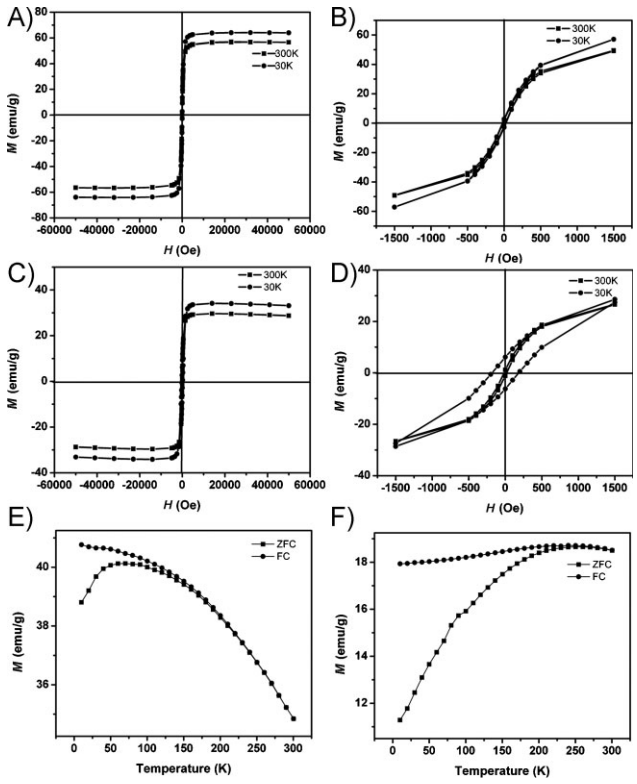

Figure 5. Plots of magnetization versus applied field obtained at 30 and 300 K, respectively, for A) Fe_3O_4 NPs and C) SiO_2-composite nanotubes containing Fe_3O_4 and CdSe. B,D) Magnified views of the hysteresis loops in (A) and (C), respectively. Temperature dependence of the magnetic susceptibility for E) Fe_3O_4 NPs and F) SiO_2-composite nanotubes containing Fe_3O_4 and CdSe, showing ZFC (closed square) and FC (closed circle) curves, with an applied magnetic field set at 500 Oe.

compared with the Fe_3O_4 NPs alone at both temperatures. Specifically, the saturation magnetization values at 30 K were 64 and 34 emu g^{-1} for the Fe_3O_4 NPs and Fe_3O_4/CdSe silica-based composite, respectively, while the corresponding values at 300 K were 57 and 29 emu g^{-1}. This observed reduction could be attributed to the normalization of the magnetization to the total mass of the composite including the CdSe QDs and SiO_2 nanotubes. Thus, the magnetic contribution from the Fe_3O_4 NPs was underestimated. A similar reduction of the saturation magnetization has been previously observed with Fe_3O_4/CdS bifunctional nanocomposites.[33,34]

The zero-field-cooled (ZFC) and field-cooled (FC) magnetization measurements subject to an applied field of 500 Oe are shown in Figure 5E and F. The ZFC and FC curves coincide at high temperatures but start to separate at blocking temperatures corresponding to 50 and 200 K for magnetite and silica-encapsulated magnetite, respectively. The large difference in the blocking temperature can explain the reduced coercive field of the bare Fe_3O_4 NPs at 30 K as compared with that of the composite (Figure 5B and D). Indeed, 30 K is well below the blocking temperature of 200 K for the composite but is very close to the blocking temperature of 50 K for bare, individual NPs. The size distribution (12–14 nm) of bare Fe_3O_4 NPs implies that smaller particles would have a lower blocking temperature. Hence, at 30 K, some of them are already in the superparamagnetic state with zero coercivity, whereas all of the immobilized Fe_3O_4 NPs in the silica-based composite are definitely blocked at 30 K and possess a nonzero coercive field.

We note that such a large observed difference in blocking temperature is a rather surprising result considering the equal sizes of the magnetite NPs in each sample. The blocking temperature (T_B) of magnetic NPs is related to the energy barrier, ΔE, separating two easy (i.e., preferred) directions of magnetization via Arrhenius's law,[42] that is, $T_B \approx \Delta E/25k_B$, where k_B is the Boltzmann constant. For noninteracting NPs, the energy barrier is $\Delta E = KV$, where K is the anisotropy constant and V is the volume of a NP. The dipole–dipole or exchange interactions between NPs with an energy E_{int} increase the energy barrier, $\Delta E = KV + E_{int}$, as well as the blocking temperature of interacting NPs.[43,44] Thus, a significant increase in the blocking temperature of the silica-encapsulated CdSe/Fe_3O_4 composite strongly suggests the presence of non-negligible interparticle interactions in this sample.

In order to examine the effect of magnetic interactions, we estimated the anisotropy constant, K, for Fe_3O_4 NPs using Arrhenius's law for noninteracting NPs, namely $K \approx 25k_B T_B/V$. Using $T_B = 50$ K and assuming that particles are spheres with an average diameter of 14 nm, the anisotropy constant K was computed to be 1.2×10^4 J m^{-3}. This value is in an excellent agreement with the anisotropy constant of the bulk magnetite, $K_{bulk} = 1.3 \times 10^4$ J m^{-3}.[45]

The fact that the anisotropy constant of our particles is similar to its bulk counterpart is not surprising if their relatively large diameter of 14 nm is taken into account. The anisotropy of a NP significantly increases from its bulk value with decreasing particle size because of the emergence of an additional surface anisotropy. In the case of Fe_3O_4 NPs, it is generally increased by an order of magnitude for particles with a diameter in the range 4–7 nm.[46,47] The fact that the energy barrier of Fe_3O_4 NPs is consistent with the expected value for noninteracting NPs suggests that the effect of magnetic interactions was reduced by dilution in paraffin. For bare Fe_3O_4 NPs, the dilution in paraffin presumably increased the interparticle distances and, as a result, weakened the resulting magnetic interactions. By contrast, in the Fe_3O_4/CdSe silica-based composite, the distance between individual Fe_3O_4 NPs remained relatively intact upon dilution because the particles are immobilized due to attachment to the silica nanotubes. Hence, while the distance between silica nanotubes can surely be modified with dilution, the spatial separation between individual Fe_3O_4 NPs within the tubes remains unaffected.

Interactions between NPs can also explain the difference in the coercive fields of both samples. The 180 Oe coercive field of the composite at 30 K is still larger than the highest coercive field of 100 Oe observed at 5 K in bare NPs (Figure S8). Such an increase in the coercive field is consistent with an increase in the magnetic anisotropy of the NPs in the composite due to interparticle interactions. As was previously reported, those interactions not only increase the blocking temperature, but also enhance the coercive field of the magnetite NPs.[48,49]

Thus, we can conclude that the blocking temperature of the Fe_3O_4/CdSe silica-based composite is noticeably increased due

small NANO MICRO

to magnetic interactions between discrete Fe_3O_4 NPs incorporated within the silica nanotubes. In other words, our silica nanotubes create a higher confined density of magnetic NPs immobilized within their 1D structure, which invariably concentrates and strengthens the local magnetic interactions, thereby explaining the nature of our results.

2.3. Biological Perspective

To demonstrate the capability of our SiO_2-encapsulated composites as fluorescent probes, confocal microscopy images were taken, as shown in Figure 6. Figure 6A shows a typical phase-contrast image of the nanotube-composite suspension in phosphate-buffered saline (PBS), highlighting its morphological profile within the field of view. We inferred from our previous characterization data that our composites contain encapsulated CdSe NPs. Hence, we excited our sample at 488 nm and noted an emission at ≈520 nm (Figure 6B), as expected, which therefore yielded a readily detectable green fluorescence in spite of the relatively low concentration of QDs present, thus implying the inherent sensitivity of our material. The superimposition of the phase contrast and the corresponding fluorescence image data in Figure 6C is indicative of a very strong overlap and correlation, strongly suggesting that the observed optical signal likely originated from CdSe incorporated within the SiO_2-nanotube matrix itself. As a control experiment, based on an analogous superposition of phase and fluorescence data, we noted that SiO_2 nanotubes associated with Fe_3O_4 NPs alone did not appear to show any such fluorescence, even under identical imaging conditions (Figure 6D).

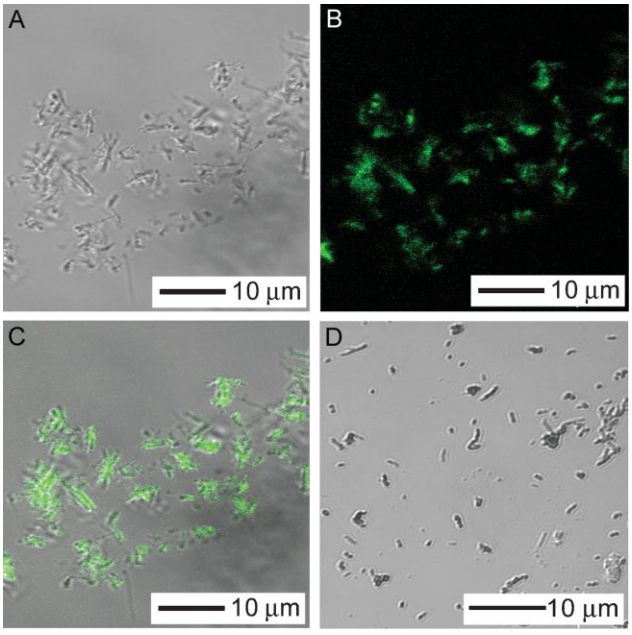

Figure 6. Confocal microscopy image characterization of silica-encapsulated nanotube composites containing both Fe_3O_4 and CdSe nanocrystals: A) phase-contrast image, B) fluorescence image, and C) superimposition of both (A) and (B). Control sample: D) Superimposition of phase-contrast and fluorescence images of silica-encapsulated nanotubes incorporating Fe_3O_4 alone. The data implies that neither the Fe_3O_4 NPs nor the silica nanotubes alone showed any noticeable fluorescence under identical imaging conditions.

It should be noted that, prior to all of the subsequent biology experiments, we sonicated our initial composite nanotubes for 12 h to yield smaller, more biologically relevant, and intact structures (Figure S9), measuring 1 ± 0.75 μm in length. Hence, to analyze their functional potential within a biomedical context, we further incubated our externally hydrophilic SiO_2-nanotube composites with HeLa cancer cells. We studied their cellular uptake/internalization, which likely could be attributed to endocytosis,[50] especially if the external silica surface was positively charged,[51] using confocal microscopy. Cell membranes were stained with the red dye conjugate (Texas Red-X) of wheat germ agglutinin (TR-WGA) for enhanced visualization. Figure 7A suggests that the nanotubes (highlighted in green) could indeed become internalized into HeLa cells after overnight incubation. As a control experiment, HeLa cells, which had not been exposed to any CdSe-containing silica-nanotube composites, did not show any green fluorescence whatsoever under identical experimental conditions (Figure 7B).

To confirm the spatial localization of nanotubes within a typical cell, we obtained a series of *z*-stack images of the cell (e.g., top to bottom) at 1-μm "slice" intervals (Figure S10). CdSe-containing silica-nanotube composites showed a green fluorescence that became apparent at slice 4 but had faded in intensity by slice 9. We focused on the middle slice (5) situated in the cellular interior. Data corresponding to orthogonal *x*, *y*, and *z* planes within the cell interior are shown in Figure 7C. Specifically, the main, central portion of Figure 7C corresponds to fluorescence data measured in a plane in the *z* direction, whereas the rightmost and uppermost edge regions of the image present data at planes in the *x* and *y* directions, respectively. Because these three

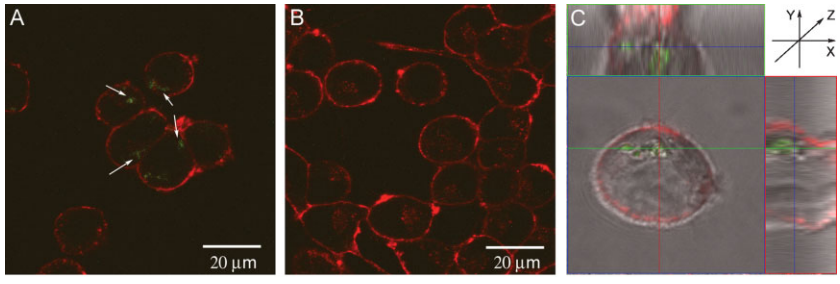

Figure 7. Confocal microscopy image characterization under identical conditions of HeLa cancer cells subjected to various treatments: A) in the presence and B) in the absence of silica-encapsulated nanotube composites containing Fe_3O_4 and CdSe nanocrystals. The cell membrane was stained red with TR-WGA conjugates. Incidence of silica-encapsulated nanotube composites containing Fe_3O_4 and CdSe nanocrystals, which fluoresce green, is suggested by the presence of white arrows in (A). C) Superposition of phase-contrast as well as red and green fluorescence images of an individual HeLa cell in the presence of nanotubes. This representative single orthogonal slice (slice 5), taken from a stack of collected 3D images (*z* stacks), as shown in Figure S10, strongly suggests that the nanotubes were incorporated within the cells.

planes share a common focal center within the cell itself and, moreover, as these intimately interconnected planes evidently all demonstrate green fluorescence simultaneously, we can reasonably conclude that the CdSe-containing silica-nanotube composites are localized (and can therefore theoretically transport cargo) within the interior of the HeLa cells themselves. Moreover, because the green fluorescence attributable to the nanotube was essentially observed only in the middle slices, as opposed to the end slices corresponding to the external cellular surfaces, our data are consistent with the nanotubes actually being internalized within the cells themselves.

Any practical biomedical device necessitates not only cell biocompatibility and penetrability, which we have discussed above, but also solubility in a biologically relevant medium. To deal with this latter issue, we took advantage of the robust chemistry of the outer silica shell of our nanocomposite. Specifically, as alluded to earlier, we grafted 3-aminopropyl triethoxysilane (APTES) onto its exterior surface (see Supporting Information). This protocol increased the dispersibility of our samples in water (Figure S11), yielding a stability of up to 24 h at a concentration of 0.5 mg mL^{-1}.

3. Conclusions

In conclusion, we have generated a novel multifunctional 1D nanostructure incorporating CdSe QDs and Fe_3O_4 NPs within a SiO_2-nanotube matrix. The intrinsic flexibility of the approach lies in the fact that the composition, shape, and size of our QD and NP building blocks can be predetermined in independent synthetic steps so as to obtain a tailored nanocomposite with rationally designed optical and magnetic properties coexisting simultaneously. In particular, the room-temperature superparamagnetism of our designed nanomaterials renders them useful for biomedical applications since they can be efficiently separated under the application of an external magnetic field. Moreover, the SiO_2-nanotube matrix is a worthy candidate as a nanoscale biomedical device, not only due to its prior and effective use[17,18,21] in bioseparation, drug delivery, and biocatalysis, but also because of its unique surface chemistry, in which its interior and exterior can be differentially functionalized with carefully chosen, complementary functionalities including, potentially, drug candidates.

4. Experimental Section

Our own synthesis route is depicted in Scheme 1. The SiO_2 nanotubes were prepared by a previously described sol–gel template method.[40] Though we cannot completely rule out the formation of nanowires and amorphous NPs, our results are consistent with the predominant production of the tubular motif, as had been reported. Briefly, anodized alumina oxide (AAO, Whatman) membranes possessing uniform, cylindrical 200-nm-diameter pores were used as templates for the fabrication of our 1D nanomaterials. An initial SiO_2 sol solution was produced by mixing tetraethyl orthosilicate (TEOS, 98%, Aldrich), H_2O, ethanol (EtOH, 99.5%, Acros), and HCl (37%, EMD) in a molar ratio of 1:4:20:0.03. The AAO membrane was then immersed in the sol for 1 h. After drying at room temperature for 1 d, the SiO_2-gel-containing template was annealed at 400 °C for 24 h so as to finally yield SiO_2 nanotubes within the alumina pores. The importance of the annealing step at 400 °C cannot be over emphasized. Whether it's due to either a lack of annealing or a lower annealing temperature, difficulties in selectively removing the AAO template in subsequent steps were encountered. Hence, this intermediate annealing step likely increased both the crystallinity and resistance to later NaOH etching of our samples, rendering it possible to devise optimal experimental conditions to specifically destroy the alumina template without simultaneously attacking the silica-nanotube motif incorporating both iron oxide and QD nanocrystals.

In theory, to selectively functionalize the interior walls of the silica nanotubes with a hydrophobic C_{18} surface, the silica-nanotube–alumina-membrane composite was immersed for 30 min in a 5% *n*-octadecyltrichlorosilane (OTS, 95 v/v%, Alfa Aesar) solution in hexane (95%, Acros).[50] This spatially localized derivatization procedure works primarily because the silane molecules could not easily attach to the outer SiO_2-nanotube surface for steric reasons. After all, the external SiO_2 wall was itself in direct contact with the alumina pore channel and therefore was physically inaccessible and otherwise "masked".[18] We necessitated this hydrophobically tuned interior in order to facilitate the incorporation of a significantly higher percentage of subsequently added NPs than otherwise would have been expected by taking advantage of the capillary effect alone.

For the purposes of this paper, our modifications of the well-known syntheses of 3–4-nm CdSe QDs[52] and 12–15-nm Fe_3O_4 NPs[53] are separately described (see Supporting Information), although the point is that purified nanoparticulates of any size could, in theory, have been readily generated and used in these experiments. TEM images of our as-prepared CdSe QDs and Fe_3O_4

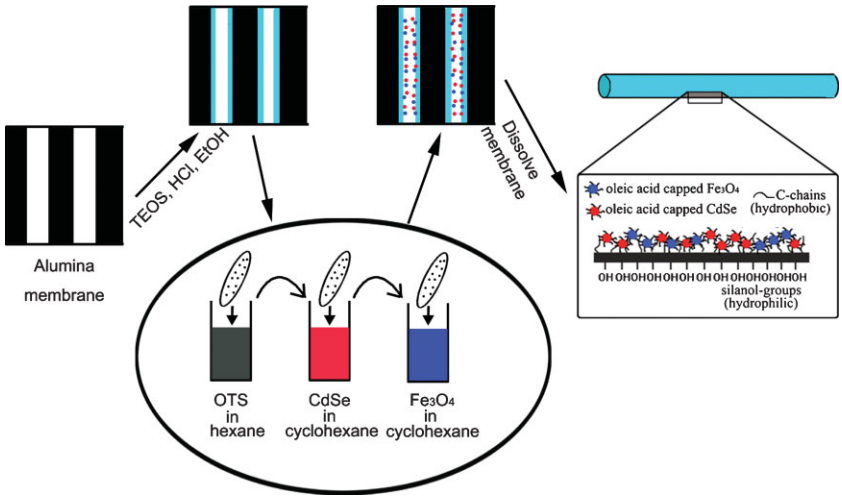

Scheme 1. A plausible synthesis route for the creation of multifunctional silica-encapsulated composite nanostructures.

NANO MICRO small

NPs are shown in Figure S1. Upon washing with hexane to remove excess OTS, our as-formed silica-nanotube–alumina-membrane composite was initially immersed in a cyclohexane solution containing QDs (10 mM) for 24 h. Then, after washing with cyclohexane to remove unbound CdSe QDs, the membrane composite was immersed in a cyclohexane solution containing NPs (100 mM) for 24 h. We noted that the precise sequence of immersion for the silica-nanotube–alumina-template composite with respect to the individual solutions containing the QDs and NPs could be interchanged without significant alteration in the resultant product. Finally, the composite was washed with cyclohexane and dried at room temperature for 1 d prior to removal of the alumina template itself by treatment with 1.25 M NaOH for 1.5 h, which, as we fully describe in the Supporting Information and Figure S2, turned out to be the most optimized conditions for isolating intact samples while maintaining both their structural and chemical integrity.

Silica-encapsulated composite samples were collected after centrifugation, washing, and drying steps. Figure S3 highlights the importance of the OTS treatment of the SiO_2-nanotube–alumina-membrane composite. In the derivatized analogues, we have a clear visual confirmation of NP inclusion upon immersion of the composite in the colored NP solutions. Conversely, the use of an unmodified silica-encapsulated composite yields results that resemble control experiments, wherein little discoloration (and therefore NP incorporation) of the sample is observed.

Acknowledgements

Research carried out (in whole or in part) at the Center for Functional Nanomaterials at Brookhaven National Laboratory was supported by the U.S. Department of Energy, Office of Basic Energy Sciences under Contract No. DE-AC02-98CH10886. M.C.A. and S.S.W. specifically acknowledge the U.S. Department of Energy (DE-AC02-98CH10886) for facility and personnel support for work completed in the Condensed Matter Physics and Materials Science Department. S.S.W. also acknowledges the National Science Foundation (CAREER Award DMR-0348239) and the Alfred P. Sloan Foundation for PI support and experimental supplies. The authors also thank Dr. James Quinn and Dr. Susan van Horn at SUNY Stony Brook for their invaluable help with electron microscopy measurements.

[1] X. Michalet, F. F. Pinaud, L. A. Bentolila, J. M. Tsay, S. Doose, J. J. Li, G. Sundaresan, A. M. Wu, S. S. Gambhir, S. Weiss, *Science* **2005**, *307*, 538.
[2] S.-J. Park, T. A. Taton, C. A. Mirkin, *Science* **2002**, *295*, 1503.
[3] N. R. Jana, C. Earhart, J. Y. Ying, *Chem. Mater.* **2007**, *19*, 5074.
[4] W. Zhao, J. Gu, L. Zhang, H. Chen, J. Shi, *J. Am. Chem. Soc.* **2005**, *127*, 8916.
[5] J. Kim, H. S. Kim, N. Lee, T. Kim, H. Kim, T. Hu, I. C. Song, W. K. Moon, T. Hyeon, *Angew. Chem. Int. Ed.* **2008**, *47*, 8438.
[6] P. Mulvaney, L. M. Liz-Marzan, M. Giersig, T. Ung, *J. Mater. Chem.* **2000**, *10*, 1259.
[7] M. A. Correa-Duarte, M. Giersig, L. M. Liz-Marzan, *Chem. Phys. Lett.* **1998**, *286*, 497.
[8] M. Alejandro-Arellano, T. Ung, A. Blanco, P. Mulvaney, L. M. Liz-Marzan, *Pure Appl. Chem.* **2000**, *72*, 257.
[9] A. Ulman, *Chem. Rev.* **1996**, *96*, 1533.
[10] E. Ruckenstein, Z. F. Li, *Adv. Colloid Interface Sci.* **2005**, *113*, 43.
[11] D. Muller-Schulte, T. Schmitz-Rode, P. Borm, *J. Magn. Magn. Mater.* **2005**, *293*, 135.
[12] C. Earhart, N. R. Jana, N. Erathodiyil, J. Y. Ying, *Langmuir* **2008**, *24*, 6215.
[13] L. Li, E. S. G. Choo, Z. Liu, J. Ding, J. Xue, *Chem. Phys. Lett.* **2008**, *461*, 114.
[14] M. Bruchez, M. Moronne, P. Gin, S. Weiss, A. P. Alivisatos, *Science* **1998**, *281*, 2013.
[15] A.-H. Lu, E. L. Salabras, F. Schuth, *Angew. Chem. Int. Ed.* **2007**, *46*, 1222.
[16] Y. Chan, J. P. Zimmer, M. Stroh, J. S. Steckel, R. K. Jain, M. G. Bawendi, *Adv. Mater.* **2004**, *16*, 2092.
[17] S. J. Son, J. Reichel, B. He, M. Schuchman, S. B. Lee, *J. Am. Chem. Soc.* **2005**, *127*, 7316.
[18] D. T. Mitchell, S. B. Lee, L. Trofin, N. Li, T. K. Nevanen, H. Soderlund, C. R. Martin, *J. Am. Chem. Soc.* **2002**, *124*, 11864.
[19] C.-C. Chen, Y.-C. Liu, C.-H. Wu, C.-C. Yeh, M.-T. Su, Y.-C. Wu, *Adv. Mater.* **2005**, *17*, 404.
[20] S. J. Son, S. B. Lee, *J. Am. Chem. Soc.* **2006**, *128*, 15974.
[21] S. J. Son, X. Bai, S. B. Lee, *Drug Discov. Today* **2007**, *12*, 650.
[22] X. Bai, S. J. Son, S. Zhang, W. Liu, E. K. Jordan, J. A. Frank, T. Venkatesan, S. B. Lee, *Nanomedicine* **2008**, *3*, 163.
[23] M. H. Huang, S. Mao, H. Feick, H. Yan, Y. Wu, H. Kind, E. Weber, R. Russo, P. Yang, *Science* **2001**, *292*, 1897.
[24] Y. Xia, P. Yang, Y. Sun, Y. Wu, B. Mayers, B. Gates, Y. Yin, F. Kim, H. Yan, *Adv. Mater.* **2003**, *15*, 353.
[25] S. Mitragotri, *Pharm. Res.* **2009**, *26*, 232.
[26] S. E. Gratton, P. A. Ropp, P. D. Pohlhaus, J. C. Luft, V. J. Madden, M. E. Napier, J. M. DeSimone, *Proc. Natl. Acad. Sci. USA* **2008**, *105*, 11613.
[27] C. Xie, B. Liu, Z. Wang, D. Gao, G. Guan, Z. Zhang, *Anal. Chem.* **2008**, *80*, 437.
[28] R. Colorado, S. Y. Zeigler, A. R. Barron, *J. Mater. Chem.* **2008**, *18*, 1911.
[29] T. Zhai, Z. Gu, Y. Dong, H. Zhong, Y. Ma, H. Fu, Y. Li, J. Yao, *J. Phys. Chem. C* **2007**, *111*, 11604.
[30] J.-X. Wang, L.-X. Wen, Z.-H. Wang, M. Wang, L. Shao, J.-F. Chen, *Scripta Mater.* **2004**, *51*, 1035.
[31] W. W. Yu, L. Qu, W. Guo, X. Peng, *Chem. Mater.* **2003**, *15*, 2854.
[32] M. A. Correa-Duarte, M. Giersig, N. A. Kotov, L. M. Liz-Marzan, *Langmuir* **1998**, *14*, 6430.
[33] L. An, Z. Li, Z. Wang, J. Zhang, B. Yang, *Chem. Lett.* **2005**, *34*, 652.
[34] X. Liu, Z. Fang, X. Zhang, W. Zhang, X. Wei, B. Geng, *Cryst. Growth Des.* **2009**, *9*, 197.
[35] Y. Wang, X. W. Teng, J. S. Wand, H. Yang, *Nano Lett.* **2003**, *3*, 789.
[36] K. Yu, B. Zaman, S. Singh, D. Wang, J. A. Ripmeester, *Chem. Mater.* **2005**, *17*, 2552.
[37] D. K. Yi, S. T. Selvan, S. S. Lee, G. C. Papaefthymiou, D. Kundaliya, J. Y. Ying, *J. Am. Chem. Soc.* **2005**, *127*, 4990.
[38] V. Salgueirino-Maceira, M. A. Correa-Duarte, M. Spasova, L. M. Liz-Marzan, M. Farle, *Adv. Funct. Mater.* **2006**, *16*, 509.
[39] C. Kirchner, T. Liedl, S. Kudera, T. Pellegrino, A. Munoz Javier, H. E. Gaub, S. Stolzle, N. Fertig, W. J. Parak, *Nano Lett.* **2005**, *5*, 331.
[40] M. Zhang, Y. Bando, K. Wada, *J. Mater. Res.* **2001**, *16*, 1408.
[41] H. Lee, Y. Lee, Y. K. Youn, H. B. Na, T. Yu, H. Kim, S.-M. Lee, Y.-M. Koo, J. H. Kwak, H. G. Park, H. N. Chang, M. Hwang, J.-G. Park, J. Kim, T. Hyeon, *Small* **2008**, *4*, 143.
[42] E. P. Wohlfarth, *J. Magn. Magn. Mater.* **1983**, *39*, 39.
[43] M. F. Hansen, S. Morup, *J. Magn. Magn. Mater.* **1998**, *184*, 262.
[44] C. Petit, A. Taleb, M.-P. Pileni, *Adv. Mater.* **1998**, *10*, 259.

[45] G. F. Goya, T. S. Berquot, F. C. Fonseca, M. P. Morales, *J. Appl. Phys.* **2003**, *94*, 3520.
[46] L. Balcells, O. Iglesias, A. Labarta, *Phys. Rev. B* **1997**, *55*, 8940.
[47] S. K. Si, A., T. K. Mandal, S. Gin, H. Nakamura, T. Kohara, *Chem. Mater.* **2004**, *16*, 3489.
[48] A. D. Arelaro, A. L. Brandl, E. Lima, Jr, L. F. Gamarra, G. E. S. Brito, W. M. Pontuschka, G. F. Goya, *J. Appl. Phys.* **2005**, *97*, 10J316/1.
[49] M. Wu, Y. Ma, Y. Liu, H. Bi, Q. Fang, H. Niu, Q. Chen, *Mater. Res. Bull.* **2008**, *43*, 1321.
[50] K. Okamaoto, C. J. Shook, L. Bivona, S. B. Lee, D. S. English, *Nano Lett.* **2004**, *4*, 233.
[51] A. Nan, X. Bai, S. J. Son, S. B. Lee, H. Ghandehari, *Nano Lett.* **2008**, *8*, 2150.
[52] E. M. Boatman, G. C. Lisensky, K. J. Nordell, *J. Chem. Educ.* **2005**, *82*, 1697.
[53] J. Park, K. An, Y. Hwang, J.-G. Park, H.-J. Noh, J.-Y. Kim, J.-H. Park, N.-M. Hwang, T. Hyeon, *Nat. Mater.* **2004**, *3*, 891.

Received: July 19, 2009
Revised: October 6, 2009
Published online: December 21, 2009

